ISSN No:-2456-2165 https://doi.org/10.38124/ijisrt/25nov1064

Synthesis, Structure, Morphology of Cerium Copper Strontium Hexaferrite and Study of its Antimicrobial Activity

A. Thippeswamy[1]; Dr. Mahendra Kumar C.[2]

[1]Department of PG Studies in Industrial Chemistry, Government Arts and Science College, Karwar, 581301, Karnataka, India.
[2]Department of Biotechnology, Government Arts and Science College, Karwar, 581301, Karnataka, India.

Publication Date: 2025/12/02

Abstract: Cerium-doped copper SHF ($Ce_xCu_{0.5}Sr_{0.5}Fe_{12-x}O_{19}$) nano material was synthesized by an auto-combustion method using urea fuel. The structural changes upon the substitution of cerium with M-type strontium hexaferrites were evaluated using scanning electron microscopy and FTIR. The PXRD pattern confirmed a crystalline size of 30-36 nm indicates a pure hexagonal crystal structure. Antimicrobial activity tests against *Staphylococcus aureus* a gram positive and *Pseudomonas aeruginosa* (Gram negative) bacterial strains demonstrated enhanced antibacterial efficacy in cerium-doped copper strontium hexaferrite samples, which can be attributed to the Ce-mediated redox activity, increased surface reactivity, and the potential for reactive oxygen species (ROS) generation that can be used in producing products with a broad spectrum of antimicrobial activity.

Keywords: *Auto-Combustion Method, Antimicrobial Activity, FTIR, Hexagonal Lattice and Scanning Electron Microscopy.*

How to Cite: A. Thippeswamy; Dr. Mahendra Kumar C. (2025) Synthesis, Structure, Morphology of Cerium Copper Strontium Hexaferrite and Study of its Antimicrobial Activity. *International Journal of Innovative Science and Research Technology*, 10(11), 2201-2209. https://doi.org/10.38124/ijisrt/25nov1064

I. INTRODUCTION

Nanoparticles are cornerstones of nanoscience and nanotechnology. Recent advancements in nanotechnology have opened new avenues for their application in many fields. Materials in micrometer scale mostly exhibit physical properties similar to those of bulk materials, whereas at the nanoscale, they exhibit distinctively different physical properties. The large surface-to-volume ratio and size-dependent properties affect the physical and chemical properties of nanoparticles (NPs). To explore novel physical properties, many technologies have been designed to fabricate small structures and nanomaterials. Out of different nanomaterials, many investigators have produced improved optical, magnetic, and electrical properties of spinel ferrites ($MFe2O_4$) make them a technologically valuable group of materials [B C Reddy et al 2021]. Among the different spinel ferrites, such as $CoFe2O_4$, $ZnFe_2O_4$, $MgFe_2O_4$, $BaFe_2O_4$ etc., Nickel ferrite ($NiFe_2O_4$) has shown spinel soft magnetic material and low coercivity as well as saturation magnetization also high electrical resistivity [[B C Reddy et al 2021]. Many nanomaterials finds applications in power transformers in electronics, rod antennas, microwave devices, read/write heads for high-speed digital tapes [Costa, V. Silva, D et al,. 2008], and also in gas-sensing materials. Multi-functional Nanomaterials are in high demand in biomedical applications for their good magnetic and fluorescent properties [D.K. Mishra, X. Qi, 2010].

In the present study, cerium-doped copper strontium hexaferrites with the general formula $Ce_xCu_{0.5}Sr_{0.5}Fe_{12-x}O_{19}$ (where x= 0.0, 0.01, 0.05, and 0.09) were synthesized via the auto-combustion This synthesis technique was chosen for its easy approach, low cost and high yielding nanocrystalline powders with homogeneous elemental distribution at relatively low processing temperatures. High-purity metal nitrates of strontium, copper, iron, and cerium were used as precursors, while urea acted as the energy source and mixing to facilitate an exothermic oxidation and reduction reactions. The precursor solution was heated, which spontaneously ignited to produce a fine porous powder through a combustion process. The resulting powders were calcined and sintered to enhance their crystallinity and phase purity, forming M-type hexaferrites.

The aim of this work is to investigate the effect of Ce^{3+} substitution on structural, dielectric, magnetic and antimicrobial properties of copper-substituted strontium hexaferrites. Cerium doping is expected to influence the lattice structure, grain morphology, and cationic distribution, which in turn can modify the key functional properties. The properties of synthesized molecules were studied using X-

ISSN No:-2456-2165 https://doi.org/10.38124/ijisrt/25nov1064

ray diffraction (XRD), and scanning electron microscopy (SEM) for morphological analysis. Furthermore, the antimicrobial activity of the samples was assessed against *Bacillus cereus* and *Pseudomonas aeruginosa* using standard agar well diffusion methods. The auto-combustion method is an effective and scalable route for synthesizing multifunctional hexaferrites with tailored properties. This study demonstrates that cerium doping not only modifies the physical and magnetic characteristics but also imparts notable antimicrobial activity, making these materials promising candidates for applications in high-frequency electronics, EMI shielding, microwave devices and antibacterial coatings for biomedical uses.

II. EXPERIMENTAL

➢ *Material and Methods*

The sample for the preparation of $Ce_xCu_{0.5}Sr_{0.5}Fe_{12-X}O_{19}$ nanoparticles, that is, all metal salts and organic fuels used, were of analytical grade. The metal precursors used were Iron(III) nitrate Nonahydrates $Fe(NO_3)_3 \cdot 9H_2O$ (purity 99%), Cerium nitrate hexahydrate $Ce(NO_3)_3 \cdot 6H_2O$, Strontium nitrate $Sr(NO_3)_2$, Copper (II) chloride dihydrate $CuCl_2 \cdot 2H_2O$, and urea (CH_4N_2O), purchased from Merck chemicals and Nice chemicals respectively. Characterization of nanoparticles using Fourier transform infrared spectroscopy (FTIR) spectra of all samples were recorded on a Perkin Elmer spectrometer (Model: Spectrum 2 USA) in the wave number range 4000-300 cm-1 using KBr power pressed pellets. Phase identification via X-ray diffraction (XRD) were obtained 2θ angle in the range 20-800 with scanning rate 20 per min on a Philips diffractometer (Make: Bruker, Model: d8 Advance, Germany) using Cu Kα radiation (λ= 1.5409 A0). The sample morphologies and microstructures were observed using emission scanning microscopy (ESEM, JEOI/EO/JER-639).

➢ *Synthesis of Cerium Doped Copper SHF($Ce_xCu_{0.5}Sr_{0.5}Fe_{12-X}O_{19}$) Nanoparticles*

Reagents used to synthesis of different samples were Ferric(III) nitrate Nonahydrates $Fe(NO_3)_3.9H_2O$ (purity 99%), Cerium nitrate hexahydrate $Ce(NO_3)_3.6H_2O$, Strontium nitrate $Sr(NO_3)_2$, Copper chloride dihydrate $CuCl_2.2H_2O$ and Urea (CH_4N_2O). These were used as such without any treatment. Strontium hexaferrite and its Cerium Doped derivatives, $Sr_{0.5}Ce_{0.5}Fe_{12-x}0_{19}$ (x = 0, 0.01, 0.05 and 0.09) nanoparticles were prepared through auto-combustion method. Stoichiometric ratios of Fe^{3+}, Ce^{3+}, Sr^{2+} ions in aqueous solution in cylindrical petri dish carrying the solution of redox mixture and then placed into a furnace to attain the temperature to 500 ±10°C. Reaction underwent dehydration and ignited at one spot with large amount of gas and heat released. Whole reaction was completed within four min with Eroldering process. The sintered powders were ground in a mortar and pestle and mixed with a binder, polyvinylpyrrolidone (PVP)$(C_6H_9NO)n$. The powders are compressed into pellets using die with diameter 10 mm and a thickness of about-3mm by loading a pressure of 8-106 kg/m² for 5 min. Resulting pellets were sintered in furnace at 900°C for 6h and then gradually brought down to room temperature, for obtaining significant crystallite sizes.

➢ *Bacterial Cultures of Cerium Doped Copper SHF ($Ce_xCu_{0.5}Sr_{0.5}Fe_{12-X}O_{19}$) Nanoparticles*

Bacterial pure cultures of Bacillus *cereus* and *Pseudomonas aeruginosa* were obtained from Department of Biotechnology, GAS college, Karwar. These cultures were grown in nutrient agar media (HiMedia, Mumbai, India) at 37°C. Subcultures were prepared by transferring 1 ml of this culture to 9 ml nutrient broth and cultivated for 48 h. The bacterial cells were harvested by centrifugation (1200 g, 5 min), followed by washing with saline and finally it was suspended in 9.9 ml of sterilized saline [M.Balouiri, et.al., 2016].

➢ *Growth Inhibition Assay*

Effect of Cerium doped copper SH on the growth of different bacteria was studied by the method of Jayaprakasha et al. (2003). Appropriate quantities of Cerium doped copper SH were transferred into various flasks containing 25 ml of molten medium (NA) to obtain final concentrations of 250, 500, 750, 1000 µg /mL. Growth inhibition assay was performed as per the reference [B C Reddy et al 2021] and minimum inhibitory concentration (MIC) was reported.

III. RESULT AND DISCUSSION

In this study, $Ce_xSr_{0.5}Cu_{0.5}Fe_{12-x}O_{19}$ nanoparticles were synthesized by using economical solution combustion method and calcined at 500 ◦C. For Phase purity analysis, functional group, morphology analysis and energy band gap, the synthesized sample was characterized by using the techniques such as PXRD, SEM, EDAX, FTIR and UV–Visible spectrophotometer. Synthesis was carried out as depicted in the flowchart (Fig. 1)

ISSN No:-2456-2165 https://doi.org/10.38124/ijisrt/25nov1064

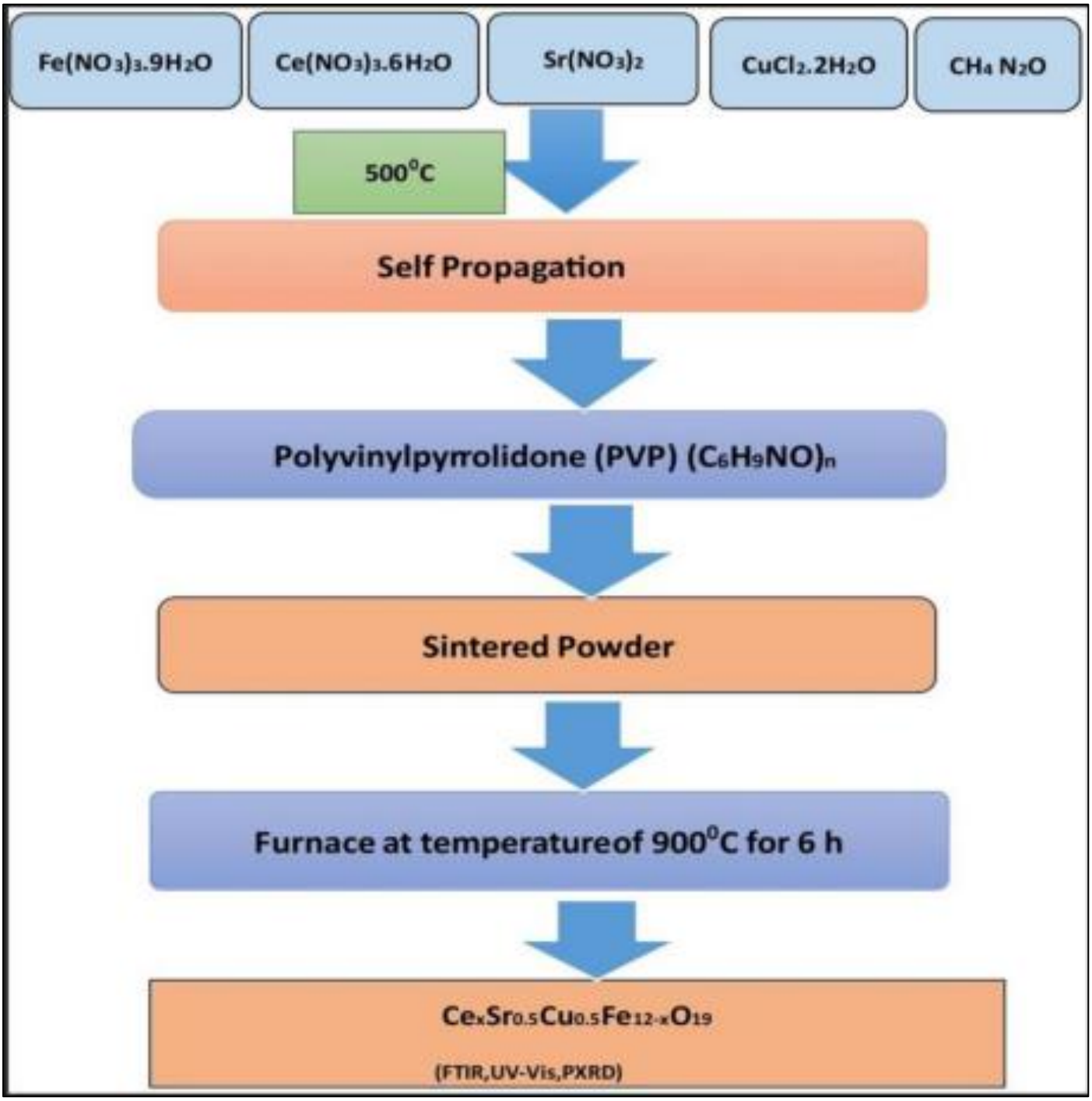

Fig 1 Synthesis, Structure Morphology of Cerium Copper Strontium Hexaferrite

➢ *PXRD Analysis*

Powder X-Ray Diffraction (XRD) analysis of $Ce_xSr_{0.5}Cu_{0.5}Fe_{12-x}O_{19}$ nanoferrites provides detailed insights into the phase composition, crystallinity, and structural evolution upon doping with cerium (Ce^{3+}). The XRD patterns of all the samples (x = 0.00, 0.01, 0.05, and 0.09) closely matched the standard diffraction data file JCPDS No. 770010 [9], confirming that all the synthesized nanomaterial was crystallized in hexagonal structure analogous to $CuSrFe_{12}O_{19}$, with no secondary phases or impurity peaks observed.

The sharp and intense peaks indicate high crystallinity, whereas peak broadening provides insights into the crystallite size. The primary diffraction peaks were indexed to the (220), (311), (222), (400), (422), (511), and (440) planes, which are characteristic of hexagonal ferrite structures [A. Thippeswamy et al., 2024].

$$\frac{1}{d^2\,\mathrm{hkl}} = \frac{4}{3}\left(\frac{h^2 + hk + l^2}{a^2}\right) + \frac{l^2}{c^2}$$

Where h, k, and l are the Miller indices, dhkl are the crystal planes, and a and c are the lattice parameters. (Fig. 2).

ISSN No:-2456-2165 https://doi.org/10.38124/ijisrt/25nov1064

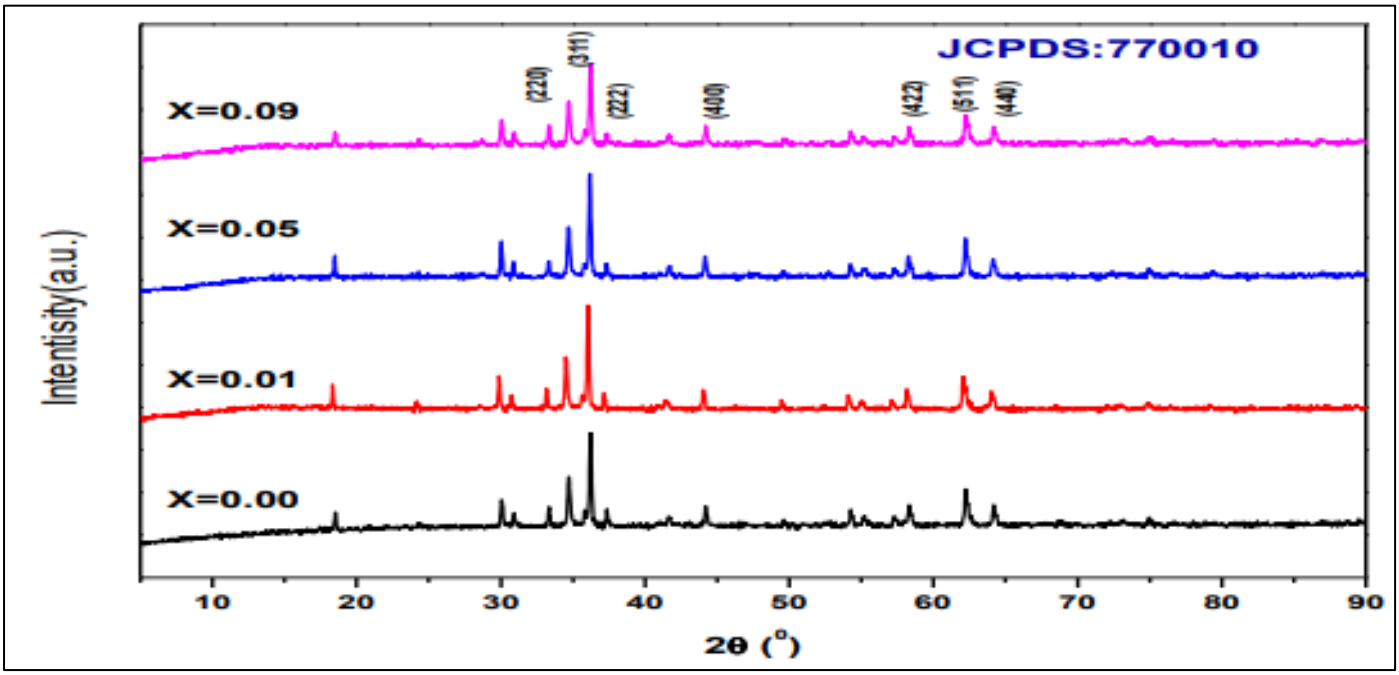

Fig 2 X-Ray Diffraction (XRD) Analysis of CexCu0.5Sr0.5Fe12-xO19 Nanoferrites

XRD studies shows there is an slight increase in lattice parameter from 0.506 to 0.509 cm^{-1} [M.Madhukara Naik, 2019], the unit Vcell of hexagonal system is determined by the relation.

$$V\ cell = 0.866\ a^2c$$

Where, a and c are lattice parameter that sustained in hexagonal system.

From the XRD profile, average size of nanoferrite crystallites was determined using Debye-Scherer equation (d) and Scherrer's formula [Boisselier E et al., 2009].

$$D = \frac{K\lambda}{\beta\cos\theta} \quad (1)$$

Here,K= 0.89 is hexagonal system constant of Scherrer's value, λ = 0.15406 nm wavelength of the incident X-rays, θ is the Bragg diffraction angle, β is the FWHM of diffraction peak. The average value of crystallite size obtained was in the range 30-40 nm and their values are tabulated in Table 1.

Hypothetical X-ray thickness (dx) of each sample was determined using the formula.

$$Dx = ZM/NV \quad (2)$$

Where Z = 2, Number of particles per unit cell, M is atomic weight, N is Avogadro's number and V is unit cell volume [Musacchio T & Torchilin VP, 2011].

The cell volume of the SrHF's patterns were set various boundaries such as a, c and v are tabulated in table1. X-ray thickness is in the range 0.506 to 0.509 cm^{-1}. Decrease in the X-ray thickness is result of doping of larger molecular weight (104.116 amu) and ion volume (0.1034 nm) of the Ce^{3+}ion can be compared to smaller molecular weight (87.62 amu) and largest ion radius (0.112 nm) of strontium ions.

Table 1 Crystallite Size (D), Lattice Constant (a & c), Cell Volume (V) and X-ray Density (ρx-ray) of $Ce_xCu_{0.5}Sr_{0.5}Fe_{12-x}O_{19}$ (x = 0.00, 0.01, 0.05 and 0.09) Nano Ferrites

Composition	Crystallite size(D)/nm	Lattice constant (a)/Å	Lattice constant (c)/Å	(c)/(a) Å	Cell volume (V)/Å	X-ray density (ρx-ray)/g cm^{-3}
$Cu_{0.5}Sr_{0.5}Fe_{12-X}O_{19}$	30.15	5.8794	22.358	3.8027	669. 57	0.521
$Ce_{0.01}Cu_{0.5}Sr_{0.5}Fe_{11.99}O_{19}$	33.25	5.8814	23.0180	3.9136	689.997	0.506
$Ce_{0.05}Cu_{0.5}Sr_{0.5}Fe_{11.95}O_{19}$	34.64	5.8814	23.0180	3.9136	689.997	0.508
$Ce_{0.09}Cu_{0.5}Sr_{0.5}Fe_{11.91}O_{19}$	36.20	5.8814	23.0180	3.9136	689.997	0.509

➢ *Fourier Transform Infrared Measurement*

The different crystal phases obtained during combustion method of prepared samples were investigated by the FTIR spectroscopy. Fig.3 show the FTIR spectra recorded for $SrFe_{12}O_{19}$ and $Ce_xCu_{0.5}Sr_{0.5}Fe_{12-X}O_{19}$ (x = 0.00, 0.01, 0.05 and 0.09) in the range of 300-4000 cm^{-1}. It was observed from the spectra that the functional group NO_3^- has been completely decomposed and thus in sintered sample, the vibrational bands of this group was n reported [Hulla, J. E., et al., 2015]. The two bands at 502 and 587cm^{-1} are observed for the hexagonal lattice and is the direct result of metal-oxygen stretching vibrations [Yang, J. J et al., 2009, Daryoush, B., & Darvish, A., 2013]. Because of various ionic vibrations in the crystal lattice of hexagonal structure, the metal ion-oxygen

ISSN No:-2456-2165 https://doi.org/10.38124/ijisrt/25nov1064

bond formation in the domain of octahedral and tetrahedral was obtained (2B).

On doping Ce^{3+}, the position of the peak slightly shifts to the lower wave number indicating replacement of Sr^{2+} by Ce^{3+} without changing the crystal structure of the composition. Further, non-existence of –OH group in the reaction product is indicated by the absence of band in the region 300-4000cm^{-1}.

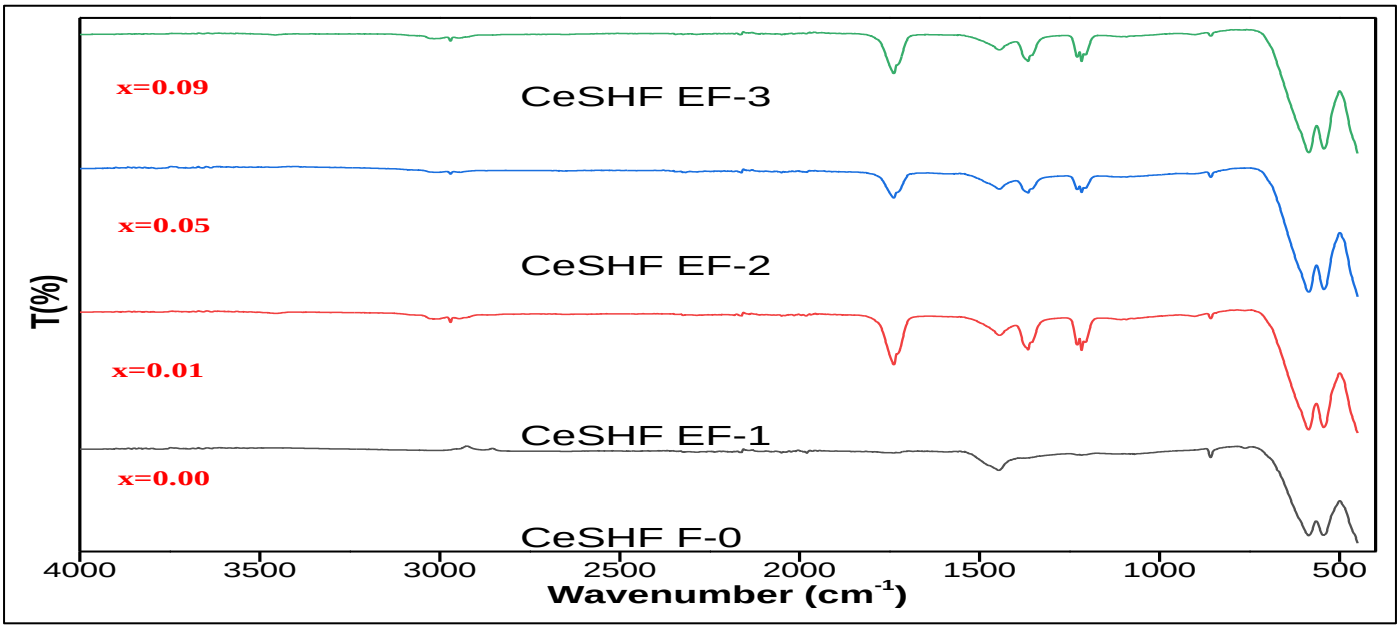

Fig 3 FTIR Spectra of Sintered Powder of $Ce_xCu_{0.5}Sr_{0.5}Fe_{12-x}O_{19}$ (x = 0.00, 0.01, 0.05 and 0.09) Nano Ferrites

➢ *Field Emmission Scanning Electron Microscopy (FE-SEM)*

The surface morphology of hexagonal $Ce_xCu_{0.5}Sr_{0.5}Fe_{12-x}O_{19}$ nanoparticles by scanning electron microscope (SEM) techniques in Figure 4. The energy dispersive X-ray (EDX) spectral studies confirmed the elemental composition of the samples [K. Elayakumar et al., 2019]. Figures 4(a,b) shows the SEM images and the Figure 4(c) shows the EDX spectra of $CexCu_{0.5}Sr_{0.5}Fe_{12-x}O_{19}$ particles with varying cerium doping concentrations. spherical and agglomerated morphology on the surface of hexaferrite $Ce_xCu_{0.5}Sr_{0.5}Fe_{12-x}O_{19}$ nanoparticles were observed. The elemental composition of the samples with varying Ce dopant was confirmed through the EDX techniques. Thus the present research showcase the extent of purity of the nanoparticles synthesized via the sol-gel route [Ahamed, M., et al., 2010].

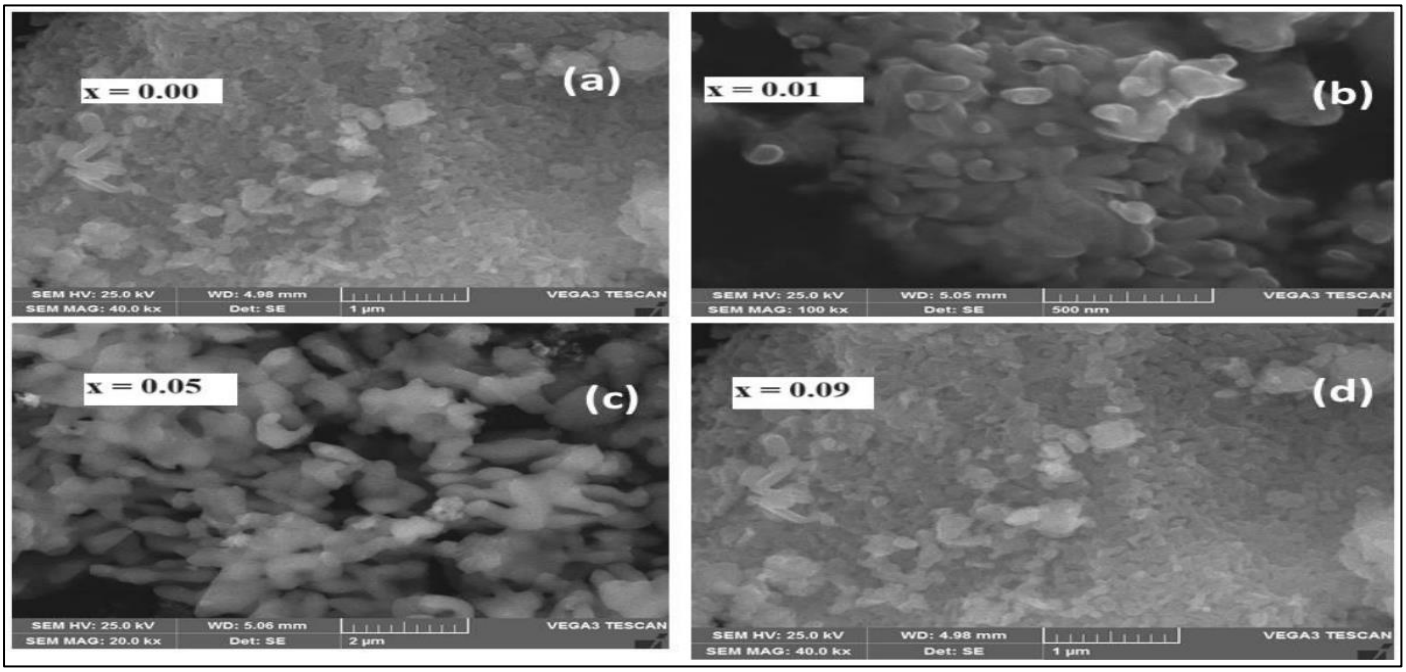

Fig 4 SEM Micrographs of M-Type Hexaferrites CexCu0.5Sr0.5Fe12-XO19 for all Compositions
(a) x=0, (b) x=0.01, (c) x=0.05 and (d) x=0.09

ISSN No:-2456-2165 https://doi.org/10.38124/ijisrt/25nov1064

IV. ANTIMICROBIAL ACTIVITY

➢ *Antimicrobial Properties of Cerium Copper SHF Nano Particles:*

Antimicrobial properties of nanoparticles were studied against both gram-positive (*Bacillus cereus*) and gram-negative (*Pseudomonas aeruginosa*) bacteria. The minimum inhibition concentration (MIC) was calculated. Viability test was conducted on two food borne pathogens: *Bacillus cereus* and *Pseudomonas aeruginosa*, table 2 and 3 shows the results of Cerium doped copper SH concentration against % inhibition bacterial growth which was carried out to determine MIC value. The results showed that as the concentration of the Cerium doped copper SH increases the viability of the organisms decreases gradually in dose dependent manner. The minimum Inhibitory concentration for the Cerium doped copper SH is 4.9 mg/ml against *Bacillus cereus* and *Pseudomonas aeruginosa* at 6.6 mg/ml concentrations (Fig. 5a and 5b). Further Investigation by using agar well diffusion assay to confirm antibacterial activity carried out. A clear zone of inhibition by the Cerium doped copper SH against *bacillus cereus* was shown in Fig. 6(a) which measures about 14 mm in size at 100 mg /mL concentration and a clear zone of inhibition by the Cerium doped copper SH against *Pseudomonas aeruginosa* was shown in Fig. 6(b) which measures about 18 mm in size at 100 mg /mL concentration.

Table 2 Effect of Cerium Doped Copper SH on *Bacillus cereus* Bacterial Growth at Different Concentrations

Substance	Quantity (mg/ mL)	No. of Colonies	% Inhibition
Control	0.00	51	0.0
Cerium doped copper SH	0.25	44	13.7
	0.50	33	35.3
	0.75	27	47.1
	1.0	22	56.9

Table 3 Effect of Cerium Doped Copper SH on *Pseudomonas aeruginosa* Bacterial Growth at Different Concentrations

Substance	Quantity (mg/ mL)	No. of colonies	% Inhibition
Control	0.00	45	0.0
Cerium doped copper SH	0.25	36	20.0
	0.50	27	40.0
	0.75	21	53.3
	1.0	15	66.7
	2.0	05	88.9

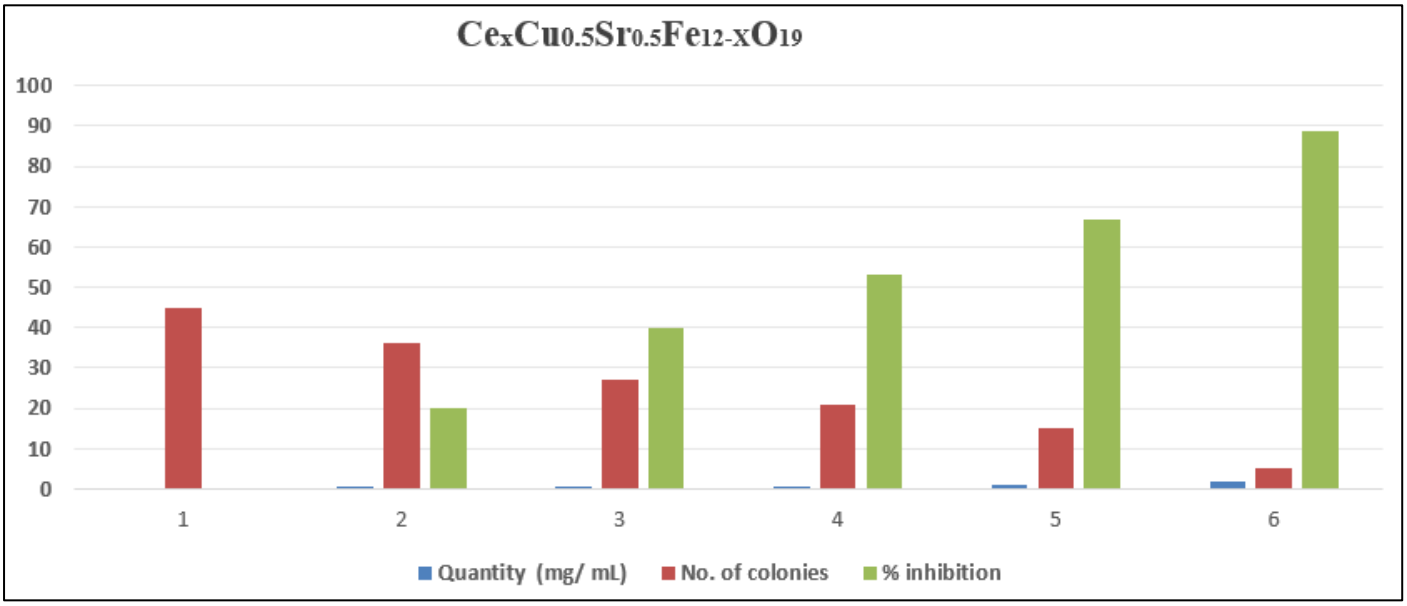

Fig 5 a) Growth of Bacillus Cereus at 0, 0.25, 0.5, 0.75, 1.0 mg /mL Concentration of Cerium Doped Derivatives

The nanomaterial showed good antimicrobial activity compared to streptomycin. The antimicrobial activity of Gold nanoparticles has been studied in both Gram-positive and Gram-negative bacteria such as *Staphylococcus aureus, Escherichia coli* and *Pseudomonas aeruginosa* [Boisselier et al]. Many reports previously of similar nanoparticles showing the antimicrobial activity of Cobalt Ferrites [M Madhukar Naik et al., 2019]. We investigated the effect of various types and concentrations of Cerium doped copper SH initially in different solvents. This study suggests that smaller sized nanoparticles have better interaction with bacterial cells. The assay can easily be used to screen a wide range of nanoparticle products. The result could also encourage us to go for further studies using lipid based

ISSN No:-2456-2165 https://doi.org/10.38124/ijisrt/25nov1064

delivery system that provide more surface to volume ratio which could increase the efficacy of antimicrobial activities reported in other similar nanoparticles [Musacchio T et al 2011]. Antimicrobial studies of cerium doped derivatives on both gram positive and negative bacterial strain was effective and it may be different in other strains of pathogenic bacteria [Takahashi N, et al 2010].

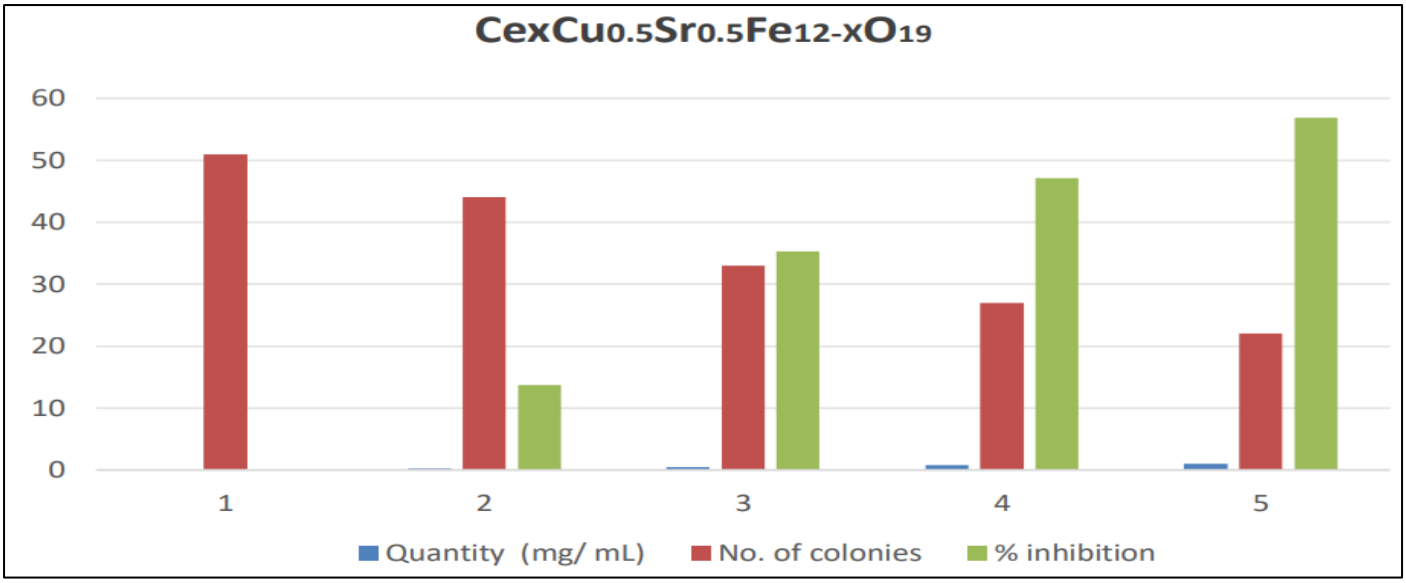

Fig 5 b) Growth of Pseudomonas Aeruginosa at 0, 0.25, 0.5, 0.75, 1.0 mg /mL Concentration of Cerium Doped Derivatives

Moreover, it needs detailed studies on the mechanism of nanoparticle action would help us better understand the function of Cerium doped copper SH affecting on these food borne pathogenic bacteria and prepare nanoparticle based pharma products in near future.

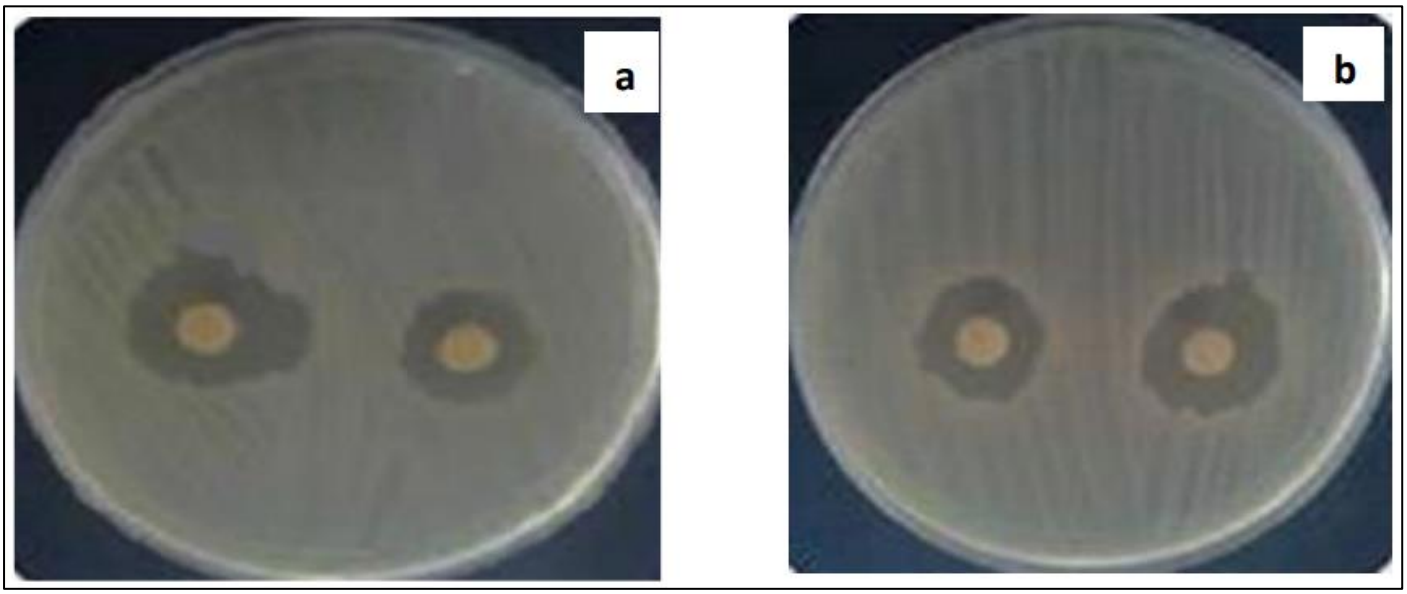

Fig 6 Bacterial Growth Suppression by Cerium Doped Copper SH Nanoparticles. Plates with Zone of Inhibition on Nutrient Agar Plates of a) Bacillus Cereus: b) Pseudomonas Aeruginosa at 100mg/mL Concentration

These molecules once absorbed will be converted in to catachol- like compounds, which could inhibit the growth of bacterial colonies. Today, multiple drug-resistant bacteria such as methicillin-resistant *Staphylococcus aureus* (MRSA), *Escherichia coli* and *Pseudomonas aeruginosa* pose a serious threat to human and animal health. Cerium doped copper SH showed the most effectiveness and could be a potential antimicrobial agent against broad spectrum of Bacteria.

V. CONCLUSION

In this study, cerium-doped copper strontium hexaferrites ($CexCu_{0.5}Sr_{0.5}Fe_{12-x}O_{19}$) were successfully synthesized via a controlled method and systematically assess the influence of Ce doping on structural, morphological, and functional properties. X-ray diffraction (XRD) analysis revealed formation of pure hexagonal M-type ferrite phase across all compositions, with no secondary phases detected,

ISSN No:-2456-2165 https://doi.org/10.38124/ijisrt/25nov1064

indicating successful incorporation of cerium ions into the crystal lattice. Observed slight shifts in diffraction peaks and the reduction in average crystallite size, as calculated using the Debye-Scherrer formula, suggested lattice distortion due to the substitution of Ce^{3+}/Ce^{4+} ions for Fe^{3+}, which may affect the local symmetry and magnetic exchange interactions. Scanning Electron Microscopy (SEM) revealed that Ce doping led to a more refined and homogeneous grain morphology, with a notable reduction in average grain size and porosity, implying that cerium acts as a grain growth suppressant and contributes to improved densification during sintering. FTIR spectroscopy provided further confirmation of structural integrity, showing prominent absorption bands in the range of 400–600 cm^{-1}, characteristic of metal-oxygen vibrations in tetrahedral and octahedral coordination sites. The slight shifts and intensity variations in these bands with increasing cerium concentration indicated modifications in local bonding environments and reinforced the XRD findings. Furthermore, antimicrobial activity tests against both Gram-positive (Staphylococcus aureus) and Gram-negative (*Pseudomonas aeruginosa*) bacterial strains demonstrated enhanced antibacterial efficacy in cerium-doped samples, which can be attributed to coordinated effects of Ce-mediated redox activity, increased surface reactivity, and the potential for reactive oxygen species (ROS) generation. These factors contribute to bacterial membrane disruption and subsequent cell death. Overall, the results demonstrate that cerium doping not only maintains the structural integrity of copper strontium hexaferrites but also significantly enhances their functional properties, particularly in terms of microstructural refinement and antimicrobial performance. This positions cerium-doped copper strontium hexaferrites as promising multifunctional materials for future applications in environmental, biomedical, and magnetic device technologies. They can be good candidate for producing pharmaceutical products that have broad spectra of antimicrobial activity.

REFERENCES

[1]. B. C. Reddy, H. Manjunatha, Y. Vidya, K. Sridhar, U. M. Pasha, L. Seenappa, C. Mahendrakumar, B. Sadashivamurthy, N. Dhananjaya, B. Sankarshan, et al., Synthesis and characterization of multi functional nickel ferrite nano-particles for x-ray/gamma radiation shielding, display and antimicrobial applications , J. Phys. Chem. Solids, 2021, 159, 110260.

[2]. Apostolov, I. Apostolova, & J. Wesselinowa, Ferrimagnetic nanoparticles for self-controlled magnetic hyperthermia. *Eur. Phys. J. B* 86, 483 (2013). https://doi.org/10.1140/epjb/e2013-40791-9

[3]. Leila Asadi Kafshgari, Mohsen Ghorbani, Asghar Azizi, Fabrication and investigation of $MnFe_2O_4$/MWCNTs nanocomposite by hydrothermal technique and adsorption of cationic and anionic dyes, Applied Surface Science, 419,2017, 70-83. https://doi.org/10.1016/j.apsusc.2017.05.019.

[4]. Costa, V. Silva, D. Cornejo, M. Morelli, R. Kiminami, L. Gama, Magnetic and structural properties of NiFe2O4 ferrite nanopowder doped with Zn^{2+}, j. Magn and Magn Mater, 2008, 320(14) DOI:10.1016/j.jmmm.2008.02.159

[5]. K. Maaz, S. Karim, A. Mashiatullah, J. Liu, M. Hou, Y. Sun, J. Duan, H. Yao, D. Mo, Y. Chen, Phys. B Condens. Matter 404 (2009) 3947.

[6]. D.K. Mishra, X. Qi, Energy levels and photoluminescence properties of nickel-doped bismuth ferrite, J. Alloys Compd. 504 (2010) 27.

[7]. M.Balouiri, M. Sadiki, Saad K. Ibnsouda. Methods for in vitro evaluating antimicrobial activity: A review, *J Pharm Anal*. 2016 Apr; 6(2): 71–79.

[8]. Jayaprakasha, Tamil Selvi, K.K. Sakariah (2003) Antibacterial and antioxidant activities of grape (Vitis vinifera) seed extracts. Food Research International 36 117–122

[9]. Clinical and Laboratory Standards Institute (CLSI). Performance Standards for Antimicrobial Susceptibility Testing. Seventeenth Informational Supplement. CLSI Document M100-S17. Wayne, USA:Clinical and Laboratory Standards Institute, 2007.

[10]. A. Thippeswamy, M.N. Manjunatha Prabhakar Chavan G . Krishnamurthy Synthesis, Structural, Magnetic, And Electrochemical Properties of Er-Ni Doped Strontium Nanoferrites, 16, 11, 2024, 1026-1045 10.22034/abec.2024.718628

[11]. Lakshmikantha, J., et al. (2022). Effect of Ce^{3+} Substitution on Sr^{2+}: Structural and Magnetic Properties of Nanocrystalline $SrFe_{12}O_{19}$. Journal of Superconductivity and Novel Magnetism, 35, 161–172.

[12]. Lakshmikantha, J., et al. (2022). Dielectric properties and magnetic behavior of Gd^{3+} substituted M-type $SrFe_{12}O_{19}$ nanoferrites. Journal of Solid-State Chemistry, 315, 123465.

[13]. Banihashemi, V., Ghazi, M. E., & Izadifard, M. (2019). (Title unavailable). Materials Science: Materials in Electronics, 30, [page number pending].

[14]. M.Madhukara Naik, H.S.Bhojya Naik , G.Nagaraju , M. Vinuth, K.Vinu, R.Viswanath Green synthesis of zinc doped cobalt ferrite nanoparticles: Structural, optical, photocatalytic and antibacterial studies, *Nano-Structures & Nano-Objects*. Volume 19, July 2019, 100322

[15]. Boisselier E, Astruc D. Gold nanoparticles in Nano medicine: preparations, imaging, diagnostics, therapies and toxicity. Chem Soc Rev. 2009;38(6):1759

[16]. Musacchio T, Torchilin VP (2011). Recent developments in lipid-based pharmaceutical nanocarriers. Front Biosci ;16:1388–412.63.

[17]. Takahashi N, Nyvad B. The role of bacteria in the caries process: ecological perspectives. J Dent Res. 2010; 90(3): 294–303

[18]. Hulla, J. E., Sahu, S. C., & Hayes, A. W. (2015). Nanotechnology: History and future. *Human & Experimental Toxicology*, 34(12), 1318–1321. https://doi.org/10.1177/0960327115603588

[19]. Yang, J. J., Pickett, M. D., Li, X., Ohlberg, D. A. A., Stewart, D. R., & Williams, R. S. (2008). Meristem

ISSN No:-2456-2165 https://doi.org/10.38124/ijisrt/25nov1064

switching mechanism for metal/oxide/metal nanodevices. *Nature Nanotechnology*, 3(7), 429–433.

[20]. Daryoush, B., & Darvish, A. (2013). A case study and review of nanotechnology and nanomaterials in green architecture. *Research Journal of Environmental and Earth Sciences*, 5(2), 78–84.Drexler, K. E. (1981). Molecular engineering: An approach to the development of general capabilities for molecular manipulation. *Proceedings of the National Academy of Sciences*, 78(9), 5275–5278. https://doi.org/10.1073/pnas.78.9.5275

[21]. K. Elayakumar, A. Manikandan, A. Dinesh, K. Thanrasu, K. Kanmani Raja R. Thilak Kumar, Y. Slimani, S.K. Jaganathan, A. Baykal (2019), Enhanced magnetic property and antibacterial biomedical activity of Ce3+ doped CuFe2O4 spinel nanoparticles synthesized by sol-gel method, Journal of Magnetism and Magnetic Materials, Volume 478, , Pages 140-147.

[22]. Ahamed, M., AlSalhi, M. S., & Siddiqui, M. K. J. (2010). Silver nanoparticle applications and human health. *Clinica Chimica Acta*, 411(23–24), 1841–1848. https://doi.org/10.1016/j.cca.2010.08.016

[23]. Mohajerani, A., Burnett, L., Smith, J. V., Kurmus, H., Milas, J., Arulrajah, A., Horpibulsuk, S., & Kadir, A. A. (2019). Nanoparticles in construction materials and other applications, and implications of nanoparticle use. *Materials*, 12(19), 3052. https://doi.org/10.3390/ma12193052

[24]. Priti A. Ingle, S. B. Kadam, Rameshwar B. Borade et al. Tailoring Structural and Magnetic Properties of Co–Zn Ferrite Nanoparticles via Erbium Substitution, 19 August 2025, PREPRINT (Version 1) available at Research Square https://doi.org/10.21203/rs.3.rs-7263499/v1